The influence of carbon nanotube buckypaper/poly (ether imide) mats on the thermal properties of poly (ether imide) and poly (aryl ether ketone)/carbon fiber laminates

Santos, Luis Felipe de Paula; Alderliesten, René; Kok, Winand; Ribeiro, Bruno; de Oliveira, Juliana Bovi; Costa, Michelle Leali; Botelho, Edson Cocchieri

DOI
10.1016/j.diamond.2021.108421

Publication date
2021

Document Version
Final published version

Published in
Diamond and Related Materials

Citation (APA)
Santos, L. F. D. P., Alderliesten, R., Kok, W., Ribeiro, B., de Oliveira, J. B., Costa, M. L., & Botelho, E. C. (2021). The influence of carbon nanotube buckypaper/poly (ether imide) mats on the thermal properties of poly (ether imide) and poly (aryl ether ketone)/carbon fiber laminates. *Diamond and Related Materials*, *116*, Article 108421. https://doi.org/10.1016/j.diamond.2021.108421

Diamond & Related Materials 116 (2021) 108421

Contents lists available at ScienceDirect

Diamond & Related Materials

journal homepage: www.elsevier.com/locate/diamond

The influence of carbon nanotube buckypaper/poly (ether imide) mats on the thermal properties of poly (ether imide) and poly (aryl ether ketone)/ carbon fiber laminates

Luis Felipe de Paula Santos [a,*], René Alderliesten [b], Winand Kok [c], Bruno Ribeiro [d], Juliana Bovi de Oliveira [a], Michelle Leali Costa [a,e], Edson Cocchieri Botelho [a]

[a] Materials and Technology Department, School of Engineering, São Paulo State University (UNESP), Guaratinguetá, Brazil
[b] Structural Integrity & Composites, Aerospace Engineering, Delft University of Technology (TU-Delft), Delft, Netherlands
[c] Toray Advanced Composites, Nijverdal, Netherlands
[d] Institute of Science and Technology, Federal University of São Paulo (UNIFESP), São José dos Campos, Brazil
[e] Lightweight Structures Laboratory, Institute for Technological Research (IPT), São José dos Campos, Brazil

ARTICLE INFO

Keywords:
Buckypapers
Electrospinning
Viscoelastic properties
Thermal analysis

ABSTRACT

The use of carbon nanotube buckypapers (BP) has boosted their use in polymeric composites. However, their low permeability makes processing difficult and limits their use. This work's essential contribution is to define the best parameters to process the buckypapers through vacuum filtration technique and the use of electrospun poly (ether imide) (PEI) mats as a substrate during the BP processing to favor matrix/nanoparticle adhesion and improving the handling. Three different sonication power (50, 75, and 100 W) were used in the buckypaper processing to evaluate its influence. From the results obtained, the chosen power was 100 W due to large pore dimensions (100-200 nm) and a more significant structural order observed through L002 (crystallite size) of 2.80. The addition of BP/PEI mats favored an increase in PEI laminates' thermal stability by increasing its initial decomposition temperature by 10 °C and an increase of 9 °C in the glass transition temperature. For poly (aryl ether ketone) (PAEK) laminates, the addition of BP/PEI mats did not impact thermal stability and melting temperature but promoted a 6 °C reduction in crystallization temperature. On the other hand, the BP without PEI mats promoted a reduction of the studied properties, which can be associated with a lousy impregnation of the matrix in the buckypaper resulting in a weak interface. DMA analyses show that BP/PEI in both laminates (PEI and PAEK) favored the interaction between the constituents and present a larger region of interphase compared to BP without PEI/mats thus optimizing the load transfer throughout the interface.

1. Introduction

Carbon fiber reinforced polymer composites (CFRP) are materials that combine low specific mass (~ 1.5 g/cm^3) and high mechanical strength (elastic modulus ~55GPa, and tensile strength of approximately 825 MPa). These properties make them attractive for applications in the aeronautical industry since the transport sector is continuously seeking to reduce the aircraft's weight, thus contributing to the reduction of fuel consumption and CO_2 (carbon dioxide) emissions [1,2]. In recent years, the two leading companies in the aircraft manufacturing sector, Boeing and Airbus, launched the 787 and A350 aircraft, respectively, in which both are made up of approximately 50% by weight of composite materials, boosting the relevance of this material in the aircraft construction [3].

The growing use of polymer composites and the continuous search for high-performance materials make nanocomposites to play a central role, as their use incorporates the concept of multifunctional materials. The material is considered multifunctional when it combines the structural function with a non-structural function. Such a concept promises significant improvements in the overall efficiency of the system through weight, volume and cost reduction, without the need for embedded or attached devices to implement a non-structural functional. Multifunctionality also enhances durability, simplifies design, and increases the functional volume. In this context, nanostructured polymer

* Corresponding author.
E-mail address: luis.santos@unesp.br (L.F.P. Santos).

https://doi.org/10.1016/j.diamond.2021.108421
Received 12 February 2021; Received in revised form 19 March 2021; Accepted 19 April 2021
Available online 24 April 2021

composites have been gaining relevance in the last two decades because they constitute the most promising materials for multifunctional applications [4,5].

The incorporation of nanoparticles dispersed in polymeric matrices is not a new concept since several researchers have already carried out studies in this area of knowledge [6–8,85]. Among the available nanoparticles to be employed in nanocomposite are the carbon nanotubes (CNT), which consist of a perfect graphene sheet rolled into a cylinder, formed by a fullerene structure hexagonal and pentagonal faces. The CNT are composed of a network of sp^2 carbon atoms in hexagonal shape, having a length of the order of micrometers (μm) and diameter in the order of nanometers (nm) [9,10]. They stand out for having high values of thermal and electrical conductivities (electrical conductivity between 10^7 and 10^8 S/m and thermal conductivity at room temperature of 1750–5800 $W.mK^{-1}$), excellent mechanical performance (elastic modulus of ~1TP and tensile strength between 11 and 63 GPa), and low specific mass (1.0–2.0 $g.cm^{-3}$) [11,12].

However, the main challenge that persists in developing nanostructured systems is the nanoparticles agglomeration during the processing of the material. CNTs tend to agglomerate during the composites' preparation due to the van der Waals forces present between the tubes, which favors agglomerates in the matrix, and consequently, generate non-homogeneous materials with physical properties below the average [13,14]. Another factor to highlight is the increase in viscosity for thermoplastic polymeric systems by adding carbon nanotubes, a consequence of the high aspect ratio of the nanoparticles. Therefore, these characteristics are still a challenge to overcome in nanostructured polymer composites [14,15].

As an alternative to the points previously mentioned, CNTs films, better known as buckypapers (BP), has been increasingly used by researchers [16–18]. BPs can be defined as thin films, with a thickness of the order of 50–100 μm, displaying a highly porous structure formed by a dense network of carbon nanotubes linked cohesively by van der Waals forces [19,20]. The homogeneous and dense morphology is obtained not only on the surface but also through its thickness [21]. However, the nanometric dimensions of carbon nanotubes favor the formation of small pores, reducing BP permeability by 8 to 10 times compared to a conventional fiber fabric, making it difficult for the polymer matrix to infiltrate during processing [22].

Poly(ether imide) (PEI) and Poly(aryl ether ketone) (PAEK) are high performance engineering thermoplastics. PEI is an amorphous polymer with a high glass transition temperature (~217 °C), it has easy processability, good chemical and hydrolytic strength, high thermal stability (its thermal decomposition starts above 450 °C), high elasticity modulus (3.2 GPa), and tensile strength (105 MPa) [23]. The aromatic rings provide high binding energy and a high glass transition temperature, enabling its use at high service temperatures [24]. On the other hand, PAEK is a semi crystalline polymer with good thermal stability, toughness, high mechanical strength, good impact strength at low temperatures, chemically inert, and biocompatible. This polymer has a glass transition temperature of approximately 157 °C and a melting temperature of 305 °C. In addition to these characteristics, it also has an ultra-low friction coefficient and good machinability, making it more attractive for the design of complex engineering shapes and parts [25].

Polymeric materials have an intense viscoelastic behavior, and in other words, they simultaneously present characteristics of a fluid and an elastic solid. Therefore, when these materials are subjected to mechanical loading, part of the energy is dissipated as heat or acoustic emission, while another part is stored as elastic energy [26].

Three-phase structural composites and their properties, particularly those with engineering thermoplastics and carbon nanotubes buckypapers, have not been fully explored because most studies focus on study two-phase composites (polymer and nanoparticle) composed by thermoset matrix and nanoparticles are usually dispersed in the matrix. The four main benefits of adding carbon nanotubes buckypapers in fiber-reinforced thermoplastic composites can be summarized as: 1) BP laminates are manufactured by simple processing techniques, such as hot compression molding, avoiding more complex and expensive processes such as autoclave [27]; 2) vacuum filtration for obtaining BPs is considered a low-cost technique that makes it possible to obtain BPs in large dimensions, thus expanding the range of applications and improving safety in the use of carbon nanotubes on a large scale [20]; 3) CNT concentration in the laminate can easily surpass 20% in volume, showing more significant gains than conventional CNT polymer composites in properties such as thermal stability and viscoelasticity [28], besides avoiding the problems of agglomeration and increased viscosity in composites with CNTs dispersed in the matrix.; 4) The use of PEI mats in the present work, aims to improve the handling of BPs, as they are fragile by itself, and can solve the problem of low permeability of BPs, therefore favoring interfacial adhesion with the viscous matrix and fibers later. PEI mats can also favor composites toughening after their addition [29,30].

The excellent thermal properties of carbon nanotubes impact BP-based composites' properties, such as thermal stability and viscoelasticity. Thermal stability is crucial to define the application temperature and the dimensional stability of the material [31]. Some studies show the effectiveness of BPs in gaining thermal stability, such as the study carried out by Díez-Pascual [28] and co-workers. They showed an improvement in this property, since the addition of BP in the PEEK polymer (poly (ether ether ketone) promoted an increase of 30 °C in the initial degradation temperature. Similar behavior was observed by Ribeiro et al. [31] in which the incorporation of BP promoted a gain of 35 °C in the initial temperature of thermal decomposition. These increases are attributed to the high thermal conductivity of CNTs favoring the transport of heat through the phonons and increasing the barrier effect that hinders the diffusion of products associated with degradation.

Viscoelasticity is also an essential property that allows characterizing the polymer systems' usability, especially for composite materials. This property is normally studied through dynamic mechanical analysis (DMA), so this technique allows evaluating the interfacial behavior and adhesion nature that will help to understand the BPs contribution in the performance of the composite [32]. The carbon nanotubes network, which is characteristic of buckypapers, can favor the stress transfer and interfacial adhesion between the matrix and nanoparticle. Also, can restrict the polymeric chain's mobility in the regions adjacent to the BPs, therefore promoting improvements in the viscoelastic properties of the material [33].

In this work, the carbon nanotube buckypapers will be processed via vacuum filtration with three different sonication powers (50, 75, and 100 W). Later, their morphology, porosity, presence of defects, and crystalline structure will be evaluated to determine the best processing conditions. Subsequently, PEI mats will be processed through electrospinning, aiming to overcome the BP's low permeability, thus favoring the BP/semipreg interfacial adhesion and BP handling. Also, the influence of BP with and without PEI mats on thermal stability, melting and crystallization temperatures and the viscoelastic properties of PEI and PAEK laminates were studied. It is noteworthy that the incorporation of carbon nanotube buckypapers in high-performance thermoplastic composites reinforced with carbon fibers has been little explored, thus this work also aims to contribute.

2. Experimental

2.1. Materials

Multi-walled carbon nanotubes (MWCNT-Nanografi) were synthesized by chemical vapor deposition showing >92% purity. The MWCNTs were functionalized with a carboxyl group (COOH) to increase the reactivity of the particles and improve the interfacial interaction between MWCNT and the matrix. The internal and external diameters were 5–15 nm and 8–10 nm, respectively, and their lengths vary from 1 to 3 μm. *triton* X-100 (surfactant) consists of a viscous/colorless liquid,

with a pH of around 6.0–8.0, a boiling temperature of 200 °C, and a specific mass of 1.07 g.cm^{-3}. Its use promotes non-covalent functionalization and assists during the dispersion of MWCNT. Poly (ether imide) was supplied by a Saudi company Sabic's Innovative Plastics, under the commercial name ULTEM 1000 and had the following properties: the specific mass of 1.27 g.cm^{-3} and glass transition temperature (T_g) of 217 °C; this polymer was used in the electrospinning of PEI mats. The solvents used in preparing the electrospinning solution were *N*-methyl-2-pyrrolidone (NMP) and dimethylacetamide (DMAC). Toray Advanced Composites TC1225 (poly(aryl ether ketone)/carbon fiber) and TC1000 Premium (poly(ether imide)/carbon fiber) semipregs were used to consolidate the composites.

2.2. Electrospinning of PEI polymeric mats

The electrospinning process was employed to produce polymeric PEI mats to be used as a substrate during the filtration step and in preparation of the buckypapers. The PAEK electrospinning was not performed once no solvent has been found in the literature that effectively solubilizes the PAEK. The electrospinning system used in this work consists of the following items: a high voltage source (0–30 kV); a collector composed of a grounded cylinder which is rotated by a geared motor (MRT910-Tekno); dehumidifier; glass syringe with a capacity of 20 mL with stainless steel fitting and stainless steel Hamilton type needle; and a thermohygrometer (Minipa-MT-241) to collect information of humidity and temperature. Firstly, 15% *w*/w PEI solution was solubilized in a mixture of *N*-methyl-2-pyrrolidone/dimethylacetamide (NMP/DMAC) in the proportion of 7:3 by volume on a magnetic stirrer at a temperature of 60 °C. Subsequently, the following parameters were used during the electrospinning of the mats: stainless steel needle of 8 mm long and 2 mm in diameter, cylinder rotation of 60 rpm, an applied voltage of 19 kV, working distance of 8 mm, air humidity of 50%, the temperature of 21 °C, and collection time of 3 h. The author's parameters used during the electrospinning process were obtained from previous tests and based on works available in the literature [34,35].

After processing the polymeric PEI mats, they had their morphology characterized by scanning electron microscopy (SEM) and the BP/PEI mats. The samples were cleaned with a nitrogen jet, covered with a thin gold layer, and subsequently evaluated by a microscope from a Zeiss model EVO LS-15. During this analysis, backscattered (BSE) signals were obtained using the Zeiss 4Q-BSD, a four-quadrant semiconductor detector, with an acceleration voltage of 5 kV PEI mat characterization and 1 kV for BP/PEI mats.

2.3. Buckypaper processing and characterization

The buckypaper (BP) fabrication was performed according to the literature [18,36,37], using the vacuum filtration technique. Firstly, 50 mg of MWCNT were dispersed in 100 mL of deionized water with 1 g of Triton X-100 performed on an ultrasonic tip of the Hielscher brand (model UP400st). After dispersing the MWCNT, the suspension was centrifuged for 30 min at 4000 rpm in a Kasvi centrifuge (model K14–4000). The suspension was vacuum filtered in a Millipore filtration system, with a nylon membrane (0.45 μm). It is essential to point out that two BP types were prepared in this work: a pure BP and BP/PEI film. BP/PEI films were prepared by stacking two layers of PEI mat over the nylon membrane previously to the filtration step. Subsequently, the BP was washed with acetone (50 mL) and isopropyl alcohol (50 mL) to remove the adsorbed surfactant molecules, and then the BP was dried in a vacuum oven at a temperature of 100 °C for 8 h. Fig. 1 shows the BP processing steps, followed by laminates processing through hot compression molding.

According to Rojas et al. [21], the dispersion time (40 min) and amplitude (40%) were defined to be used during the first step of BP fabrication to promote a well-dispersed suspension without damage to the MWCNTs structure. Thus, in this work, the influence of the ultrasound tip's power during BP processing was evaluated. Three samples were prepared at 40% amplitude for 40 min in a pulse mode (10s on and 5 s off), using power levels of 50 W, 75 W, and 100 W.

The characterizations techniques that the BP were subjected to are described as follows:

- Morphology: The BP samples were sectioned, cleaned with nitrogen jet, and their cross-section view covered with a thin gold layer (~5 nm). The samples were analyzed using a scanning electron microscope (Field Emission Gun) by Tescan model Mira 3. The images were obtained from the secondary electron beam, with a working distance of 5 mm and a current of 5 kV;

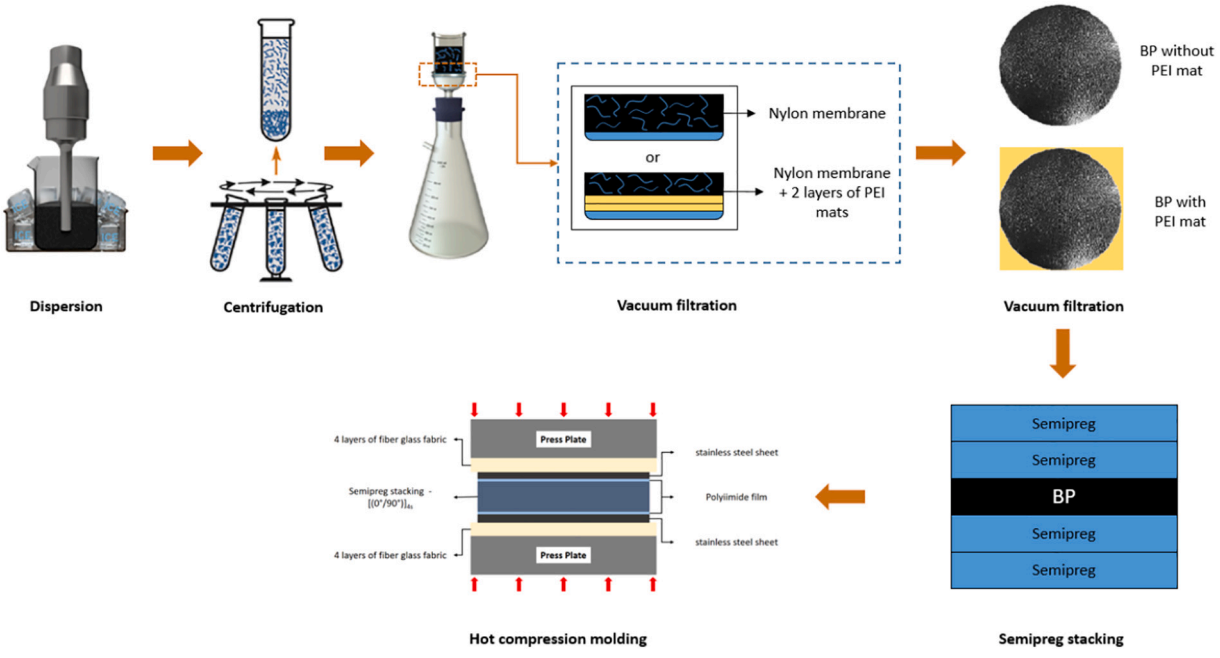

Fig. 1. Representative scheme for BP process by vacuum filtration and laminates via hot compression molding.

- Porosity: the average pore diameters were obtained from a mercury porosimeter (Quantachrome Instruments, model Poromaster). This analysis was performed at a pressure of 170 MPa and a pause time of 30 s;
- Defects: Raman spectroscopy (Horiba LabRAM HR Evolution microscope spectrometer) was used to check possible damage to the MWCNT structure during BP processing. The parameters used for this analysis were: a source of radiation excitation of 325 nm and a laser point with a diameter of 1.54 μm to identify typical dispersions of carbon structures. The spectra were recorded by scanning the region from 1000 to 1800 cm^{-1}, considering three accumulations of 30 s;
- Crystallinity: the crystallinity of the BP samples was determined by X-ray diffractometry (XRD- Bruker model V8 Advance Eco) at room temperature using a copper tube (Cu) with a wavelength of 1.5418 Å, a voltage of 40 kV, and 25 mA current. The scanning speed was 10°/min, and an angular increment of 0.01° to result in good signal quality. The diffractogram was obtained in the region of 2θ = 10–50°.

2.4. Processing and morphological characterization of processed laminates

In this work, carbon fiber reinforced polymer (PEI and PAEK) composites with BP's incorporation were processed through hot compression molding. These composites were prepared from the stacking of 4 layers of semipregs so that the BP was added in the central region in a stainless-steel mold previously prepared with the release agents Polidesmo 55 and polyimide film. The configuration obtained for these materials at the end of the process was $[0/90]_{2s}$, this configuration was based on the requirements for the future performance of mechanical tests to evaluate the influence of buckypaper on the interlaminar strength of composites. A hydraulic press (Carver, CMV100H-15-X model) was used to consolidate the laminates, and the processing parameters were: for PAEK composites, the materials were heated up to 350 °C and when reaching the temperature, a 30-min threshold was reached for temperature homogenization, a pressure of 1 MPa was applied (which was maintained until the end of processing) for 20 min and, the material was cooled to room temperature. The same parameters were used for PEI composites, except for the pressure, which was 2 MPa. The processing parameters of the materials were based on their datasheet, as well as on the Thermogravimetric analysis (TGA), dynamic mechanical analysis (DMA), and differential scanning calorimetry (DSC) analyzes previously performed on the received semipregs and polymers. In all, six sets of materials were processed, so they are PAEK/CF and PEI/CF (base laminates), PAEK/CF/BP-SM (without PEI mat), PAEK/CF/BP-CM (with PEI mat), PEI/CF/BP-SM (without PEI mat) and PEI/CF/BP-CM (with PEI mat), a scheme of these configurations is shown in Fig. 2. The content of carbon nanotubes buckypaper for each composite is approximately 3 wt%.

Subsequently, the morphology of the processed composites was analyzed to assess possible defects induced during processing, and to provide information about the BP impregnation. Samples of the cross-section of the composites were sectioned in a cutting machine with a diamond disc, cold embedded in methyl methacrylate resin, sanded with sandpaper of different particles sizes (180, 320, 1000, 2400 e 4000), and polished with a diamond paste of 6 μm, 3 μm, and 1 μm. After this preparation, the samples were analyzed in a laser optical microscope from Keyence.

2.5. Thermal characterization of processed laminates

The influence of buckypaper incorporation on the thermal properties of the processed composites was carried out using the following techniques:

- Thermogravimetric analysis (TGA): these analyses were performed based on ASTM E 1131 and E2550 standards using the equipment from SII Nanotechnology - Seiko Model TG/DTA 6200. The following parameters were used: a mass of approximately 10 mg, platinum sample holder, a heating rate of 10 °C.min^{-1}, nitrogen atmosphere with a flow of 100 mL.min^{-1}, temperature range from 25 °C to 1000 °C, and alumina as reference material;
- Differential Scanning Calorimetry (DSC): these analyses were performed according to ASTM D3418 standard, and a PerkinElmer equipment model DSC8000 was used. DSC analyses were performed in the dual scan mode: samples were heated, cooled, and then heated again. The parameters used during the analysis were: hermetic aluminum sample holder, heating and cooling rate of 10 °C.min^{-1}, nitrogen atmosphere with a flow of 20 mL.min^{-1} and a temperature range of 25 °C to 380 °C, and an approximate mass of 5 mg;
- Dynamic Mechanical Analysis (DMA): these analyzes were performed according to the procedures described in ASTM D7028 standard in equipment from SII Nanotechnology - SEIKO model DMS6100. The following parameters were used: bending mode (dual cantilever), nitrogen atmosphere under 100 mL.min^{-1} flow, the oscillation amplitude of 10 μm, frequency of 1 Hz, a heating rate of 3 °C.min^{-1}, and temperature range of 25 °C to 250 °C. The samples have dimensions of (55 × 10 × 0.7) mm. It is noteworthy that for the semipregs of PEI and PAEK, the DMA analysis was performed with the same parameters; however, in the tensile mode due to the materials' nature and thickness.

From the results of storage modulus (E'), loss modulus (E"), and Tan δ (Tan delta is often called damping), the degree of entanglement (N) and A, b, C, and r factors were calculated to study the contribution of the BP in the viscoelastic properties of processed composites. The first parameter studied was the degree of entanglement (N), which was calculated according to Eq. (1) [38].

$$N = \frac{E'}{6.R.T} \tag{1}$$

E' is the storage module at the studied temperature, R is the gas constant, and T is the absolute temperature in Kelvin.

The storage modulus represents the elastic component of the material and is associated with the material's ability to retain energy. The

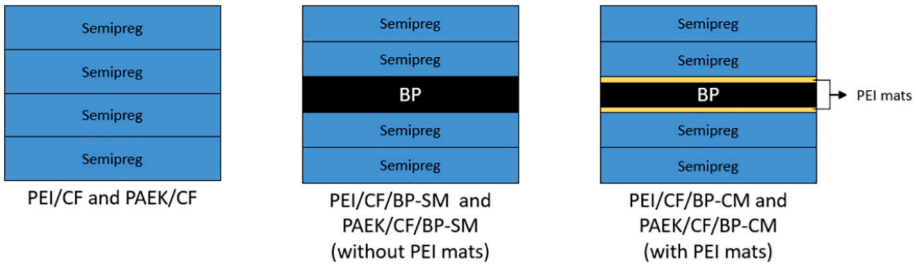

Fig. 2. Stacking configuration of processed laminates.

increase or decrease of E' from the addition of BPs is related to interfacial adhesion and the arrangement of polymer chains [39]. Thus, high N values suggest less interaction between nanoparticles, and a strong interface between the components is expected due to interfacial tension reduction [40].

The second parameter that can be calculated from E' is factor r or reinforcement efficiency factor. This factor allows the evaluation of nanoparticles' effect as reinforcement in the matrix, therefore providing information on the buckypaper bonding in the polymeric composite. This factor is calculated based on the Einstein equation (Eq. (2)).

$$E_c = E_m\left(1 + rV_f\right) \tag{2}$$

where: E_c and E_c are the composites and matrix storage modulus, respectively; V_f is volumetric fraction of nanoparticles; r is the reinforcement efficiency factor.

Another parameter that is also possible to obtain from E' is the factor C. This factor contributes to study the effectiveness of carbon nanotube buckypapers in nanostructured composites. Factor C is associated with the reduction of E' and the material passage through the glass transition temperature. The vitreous region is determined by intermolecular forces and the way the polymer chain is packaged. It is essential to mention that the higher the intermolecular forces, the greater the energy required for the transition from the vitreous to the flexible or rubbery phase [41].

Factor C is calculated from Eq. (3) [42,43].

$$C = \frac{\left(\frac{E'_v}{E'_b}\right) composite}{\left(\frac{E'_v}{E'_b}\right) neat\ material} \tag{3}$$

where: E'_v is the storage modulus in the glassy region and E'_b is the storage modulus in the flexible or rubbery region.

From tan δ, it is possible to determine factor A, also known as adhesion factor, representing the existence or the absence of possible interactions between the polymer and the nanoparticles [44]. This parameter is based on the adhesion criteria, studied and proposed by Kubát, Rigdahl, and Welander [33] so that tan δ is characterized as a function of the volumetric fraction of the constituents and it depend on the tan δ_c/tan δ_p ratio. Strong interactions occur in the composite interface, which favors the reduction of the macromolecular mobility near the nanoparticles' surface compared to the other regions of the matrix, thus reducing the value of tan δ and factor "A". Also, low values of factor "A" suggest a good interaction between the composite's constituent phases. Considering the damping of the reinforcement and interface is very low, the values in the equation are disregarded so that for the calculation of factor A, Eq. (4) is used [45].

$$A = \frac{1}{\left(1 - \phi_f\right)} \frac{tan\ \delta_c}{tan\delta_p} - 1 \tag{4}$$

where: ϕ_f is the damping of the reinforcement; c refers to the composite and p to the polymer.

A low value of A suggests a high degree of interaction/adhesion between the constituent phases; when A = 0, the interfacial interaction between the polymer and the nanoparticle was not enough to modify the adhesion, while A > 0 means that there are no interactions that are capable of reducing the macromolecular mobility of the polymer, revealing an increase in the interfacial adhesion of the laminate [40,45].

The last parameter to be analyzed is the dissipation factor that provides valuable information about the polymer and fiber interactions. In this case, damping in nanostructured polymeric composites depends on the polymer matrix and is also associated with the interactions between nanoparticles and matrix. The nanoparticle damping depends on the matrix, as it restricts the interface between the nanoparticle and the matrix and enables the formation of the interphases layer. This dissipation factor is calculated according to Eq. (5) [42,44,46].

$$\frac{tan\ \delta_c}{tan\delta_p} = \left(1 - bV_f\right) \tag{5}$$

where: V_f is the volumetric fraction of carbon nanotubes and b the correction parameter of the volumetric fraction.

The correction parameter of the reinforcement volume fraction depends on interphase layers' formation, resulting from the interactions between the nanoparticles and polymer. Thus, this factor can be interpreted in terms of interfacial adhesion between nanoparticle and polymer, considered a weak adhesion if b < 0 and strong if b > 0.

3. Results

3.1. Buckypaper processing and its characterization

As mentioned in Section 2.3, three BP samples were processed through vacuum filtration technique with the assistance of an ultrasound probe (ultrasonication), using the following parameters: 40% amplitude, 10s on and 5 s of the cycle, and processing time of 40 min, according to work published by Rojas et al. [18]. Ultrasonication technique is widely used to process carbon nanotubes buckypapers, however long time and high power can induce side wall broken, tubes shorten and amorphous carbon degradation [47]. Therefore, the ultrasound's power was varied (50, 75, and 100 W), and its influence was studied on the morphological, porosity, XRD, and Raman spectroscopy analyzes of the BP. The samples' morphology was evaluated by scanning electron microscopy (SEM), as shown in Fig. 3a, b and c.

As can be seen, the power variation showed no significant changes in the BP morphology so that the nanotubes are randomly dispersed, which suggests a good dispersion of the MWCNT. Besides, the high-powered sonication showed no damage to the nanoparticles in agreement with XRD and Raman spectroscopy analyzes. Therefore, it concluded that processed BPs are in accordance with the literature [48,49].

The porous size of the film was quantified by using a mercury porosimeter, as shown in Fig. 4a. As noted, the pores of all prepared samples have diameters up to 200 nm, a similar result compared to other works available in the literature [50,51]. Also, the increase in power promoted an increase in the pore's size. The BP1 sample (50 W) presented 58.1% of the pores with diameters <100 nm and 41.9% with diameters between 100 and 200 nm. On the other hand, BP2 (75 W) and BP3 (100 W) samples presented an average pore size between 100 and 200 nm in almost 100% of the cases. The presence of two different distributions of pore diameters for BP1 is associated with power; that is, the power of 50 W is not enough to transfer the shear forces favoring the CNT agglomerates' dispersion. Therefore, it suggests that more energy should be applied to promote the exfoliation of CNTs then promoting a stable dispersed suspension [52]. The increase in CNT films' porosity observed for BP2 and BP3 tends to favor the nanostructured composite processing since the impregnation of the BP by the polymer matrix is facilitated, contributing to obtain laminates with good physical properties.

High-power sonication is generally used to assist in the dispersion of nanoparticles, and in some extreme cases, the technique can promote damage to the CNT structure when used for long periods [14]. Therefore, to assess the density of defects or the carbonaceous structure's ordering, Raman spectroscopy is a sensitive technique that allows this kind of evaluation [16]. Raman spectroscopy was used to assess the influence of power (50, 75, and 100 W), and the results are shown in Fig. 4b. Analyzing the obtained spectra, the presence of two well-defined peaks between 1000 cm^{-1} and 2000 cm^{-1} correspond to band D and G, respectively. Also, there is a peak between 2500 cm^{-1} and 3000 cm^{-1}, associated with a second-order G' band [53,54]. The D band, which is centered at 1348 cm^{-1}, is correlated with defects in the carbon nanotube network, including sp^3 carbon hybridization, while the G band (1585

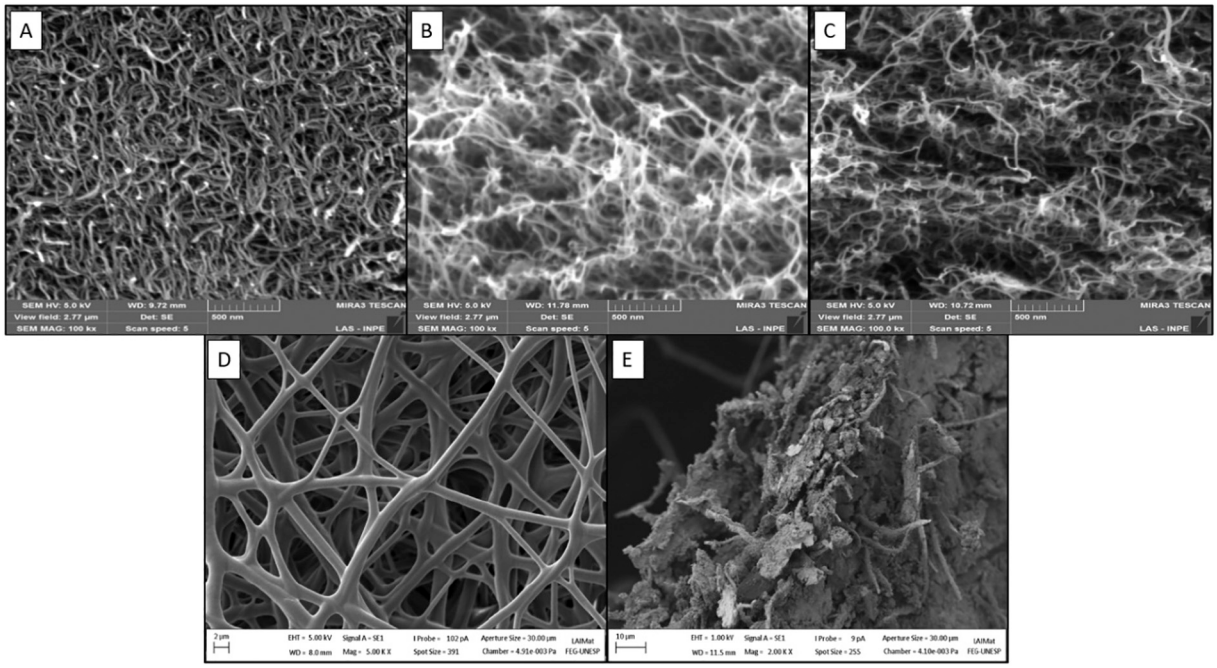

Fig. 3. Morphological images obtained through SEM of (a) BP1 (50 W), (b) BP2 (75 W) and (c) BP (100 W) with 100,000× magnification; (d) PEI mats and (e) BP with PEI/mats with 5000× and 2000× magnification, respectively.

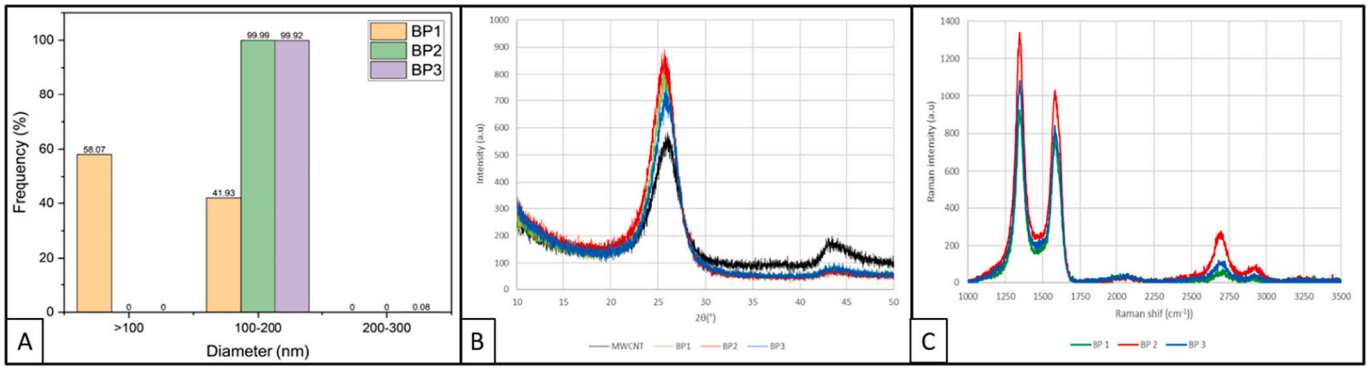

Fig. 4. (a) Porosity histogram; (b) DRX and (c) Raman spectrum obtained for BP samples.

cm^{-1}) corresponds to the tangential stretching movements of the C—C link [16,55]. The G' band is centralized at 2700 cm^{-1} and can be used to identify graphene layers [53,54]. From the obtained results, it is evident that the increase in power during BP processing promoted an increase in graphene layers, thus making the G' band more visible.

Another critical parameter, generally used for carbonaceous materials characterization, is the ratio of the intensity between D band and G band (I_D/I_G) that can be used to characterize the degree of defect in a carbonaceous material [16]. According to the spectrum obtained, the I_D/I_G ratio was 1.19, 1.33, and 1.29 for BP1, BP2, and BP3 samples, respectively, as shown in Table 1. The values obtained in this work were slightly lower than those obtained by Qu et al. [16] (2.83), Rojas et al. [18] (2.22), and Tessonnier et al. [56] who obtained an I_D/I_G value of 1.8. The lower values of the I_D/I_G ratio may be associated with some factors, such as the type of catalyst used in the nanotubes' synthesis, the low influence of sonication on the formation of damage in the nanotube structures, and a lower presence of agglomerates, which is a consequence of the functionalization process, which possibly increased the repulsive interactions between the nanoparticles contributing in the dispersion of the CNT [53,57]. Additionally, it is observed that there was no significant variation between I_D/I_G ratio for all prepared samples, which suggests that a high-power sonication was not caused significant damage to the MWCNTs structure.

Table 1
DRX and Raman spectroscopy results.

Sample	d_{002} (nm)	L_{002} (nm)	I_D/I_G
MWCNT	0.35	2.70	–
BP1	0.36	2.73	1.19
BP2	0.36	2.79	1.33
BP3	0.35	2.89	1.29

The X-ray diffractometry helps to evaluate the crystalline structure of the materials, so the reference spectra (MWCNTs) were compared to those of BP samples. The results obtained are presented in Fig. 4c. From the spectra obtained by XRD, there are two peaks, the first peak (002) being approximately at 25° associated with a graphitic material that refers to the distance between the sheets of concentric graphene that make up the MWCNTs. The second peak (100) is at 43° and is associated with the turbostratic structure (structure composed of carbon planes that resemble interlaced ribbons, with bidirectional ordering and arrangement in the third direction) [58,59] of carbonaceous materials.

From the spectra, it was possible to calculate the crystallites' dimensions that are normally expressed by the average height (L_c or L_{002}) and the average length of the layers (d_{002}). For this purpose, Scherrer's law is expressed in:

$$L_{002} = \frac{k.\lambda}{\beta.cos\theta} \quad (5)$$

and the relation between the interplanar diffraction angles and the distance between the atomic planes d_{002} is calculated with:

$$d_{002} = \frac{n.\lambda}{2.cos\theta} \quad (6)$$

The results obtained for L_{002} and d_{002} are shown in Table 1.

In both equations: λ is the wavelength of the X-ray beam, in this case for the Copper (Cu) tube, the length is 1.5418 Å; k is a proportionality constant that depends on the particle shape, ranging from 0.84 to 0.89 and for unknown geometry, the value of 0.89 must be used; β is half the height of peak 002; n is the diffraction order which is an integer 1,2 or 3, and θ is the peak diffraction angle.

The results showed that the different power sonication levels presented no impact in the distance of the atomic planes of the crystalline network of the material, a fact confirmed by the values obtained for d_{002}, which are between 0.35 and 0.36 nm. However, the use of the ultrasound tip during the BP preparation and the variation of its power promoted an increase in the crystallite size. According to Silva and Rezende [71], the L_{002} can be associated with the thickness of the CNTs walls, whereas high values of L_{002} suggest a better ordering of the graphitic structure. As can be found, the BP3 has a higher value of L_{002}, which supposes a more significant structural ordering than the other BP samples.

Based on the results presented here, the BP3 processing parameters were adopted to process the buckypapers. Although no significant variations were observed concerning morphology, porosity, and defects, this condition resulted in a buckypaper with more outstanding structural order. As observed through porosity analysis the pore size often in nanometric dimensions favors the buckypapers low permeability, which make it challenging to process nanostructured polymeric composites [18,22]. Besides, the buckypaper has a certain fragility, which often makes it challenging to handle this material [14]. Aiming to favor the handling and impregnating the BP, PEI mats were electrospun to be used as a substrate during the filtration process. The use of these mats is associated with interlayers' use to toughen the material and promote an increase in interlaminar fracture, as previously demonstrated in the literature [29,30].

The morphology of fibers processed through electrospinning is shown in Fig. 3d, and it is observed that the fibers are well defined and spaced, presenting a homogeneous distribution. Additionally, the fabricated fibers are free from defects such as drop [60] and exploded drop [61], associated with a low concentration of polymer in the solution and its viscosity. Although, in the produced material, it is possible to observe some defects of joining or fusion of fibers occurring, supposedly, due to solvent's presence in the fibers deposited in the collector, which come in contact with other, united. However, the presence of the aforementioned defect does not affect the purpose of using the mat in question. Using the open access Gwyddion software, the average fiber diameter was approximately (2.013 ± 2.921) μm.

Once the mats were processed and the best parameters for buckypaper production were defined they were used as a substrate in the vacuum filtration process of buckypapers. During the CNT film fabrication, a nylon membrane was used as a filter. On top of it, two layers of PEI mats were set, and the aqueous suspension of CNT was vacuum filtered. The tubes were randomly deposited on the filtration membrane and between the polymeric mat. The morphology of the BP with the electrospun mat is shown in Fig. 3e. As noted, BP was formed over and between PEI mats, which can be confirmed by the deposition of MWCNT in the microfibers. It was also observed that the pores present in the BP were filled with PEI fibers, which suggests better adhesion between the semipreg and the nanofilm during the composite preparation. For both composite materials prepared in this work, PEI mats were used as a substrate since the PAEK solubilization was not possible. Several studies in the polymer blend area concerning poly (ether ether ketone) (PEEK), this polymer belongs to the same family as PAEK, with poly (ether imide) (PEI). Therefore it has been proposed to use PEI mats for PAEK composites [62,63].

PEEK and PEI research available in the literature show that they are molecularly miscible, presenting only one glass transition temperature [64], and an improvement in thermal stability for the 50/50 PEEK/PEI blend has already been demonstrated by Ramani et al. [65]. Besides, as Jenkins [66] studied, the relaxation process β for PEEK was shifted to 25 °C when PEI was added, which suggests a strong molecular interaction resulting from blending miscibility. The mentioned characteristics favor the application of high-performance composites in the aeronautical field. Although the PAEK presents a similar molecular structure to PEEK, the reports concerning the influence of CNT (or BP) on PEI/PAEK blends' thermal properties are scarce, making difficult the comparison between the data obtained in this work.

3.2. Morphological characterization of nanostructured composites

The material compaction quality and buckypaper interface with the semipregs of PAEK and PEI were evaluated through optical microscopy (OM) of the cross-section of samples with dimensions of approximately (10 × 10 × 3) mm. The results obtained from the OM are shown in the micrographs of Fig. 5.

Both samples showed good compaction quality between the layers, suggesting a good percolation of the matrix in the fibers and the BP. Besides, they did not present voids, discontinuities, cracks, delamination induced during processing, or regions rich in matrix, which can negatively affect the laminate properties, suggesting that the processing parameters (temperature, pressure, and consolidation level) were adequate. Regarding BPs, it was observed that both laminates remained intact after processing, thus favoring good adhesion to semipregs, indicated by the highlighted regions of Fig. 5b, c, f, and g. From the images obtained, the thickness of the buckypaper for each laminate was measured, being 0.061 mm, 0.066 mm, 0.071 mm, and 0.088 mm for the composites PEI/CF/BP-SM, PEI/CF/BPCM, PAEK/CF/BP-SM, and PAEK/CF/BP-SM, respectively. The thickness of the buckypapers for the PEI-based composites has a smaller thickness when compared to the PAEK-based composites, and this difference may be associated with the pressure used to process these composites.

3.3. Thermal behavior of nanostructured composites

Thermal analyzes of TGA, DSC, and DMA were carried out to evaluate the influence of the addition of carbon nanotube buckypapers on the thermal behavior of the composites, and also, to trace the thermal properties of the materials studied in this work. It should be noted that DSC analysis was performed only for PAEK, a semi crystalline thermoplastic, since PEI is an amorphous thermoplastic material.

TGA analysis is a widely used technique to assess the thermal decomposition of polymeric materials due to the small amount of sample used and the possibility of carrying out analyzes in a few hours [67]. The results are presented in Figs. 6 and 7, and the data were compiled in Tables 2 and 3. Both polymer matrices studied in this work are high-performance engineering thermoplastics, which indicates that they have excellent thermal stability at elevated temperatures. The laminates, which have the PEI as a polymeric matrix, show similar thermal behaviors and possess at least one thermal decomposition step. As can be seen, the thermal decomposition of PEI/CF composite occurs between 450 °C and 800 °C, revealing an initial degradation temperature (T_i) at 470 °C, a temperature close to that of neat PEI (475 °C). It is worth

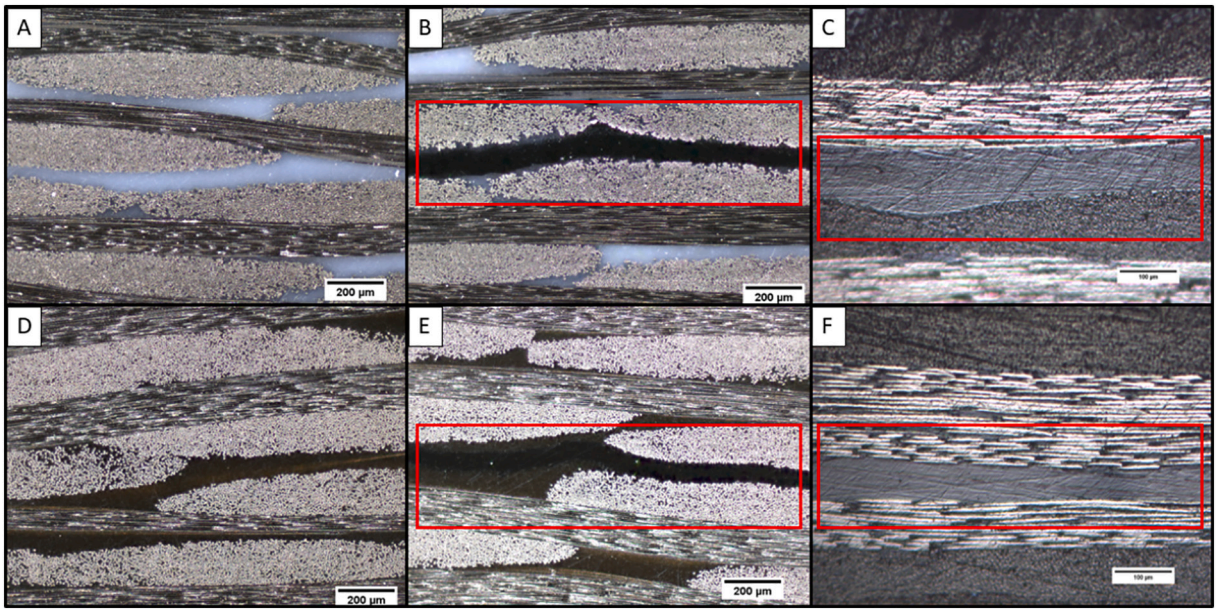

Fig. 5. Cross-section micrographs of (a) PAEK/CF, (b) PAEK/CF/BP-CM, (c) PAEK/CF/BP-SM, (d) PEI/CF, (d) PEI/CF/BP-CM, and (f) PEI/CF/BP-SM.

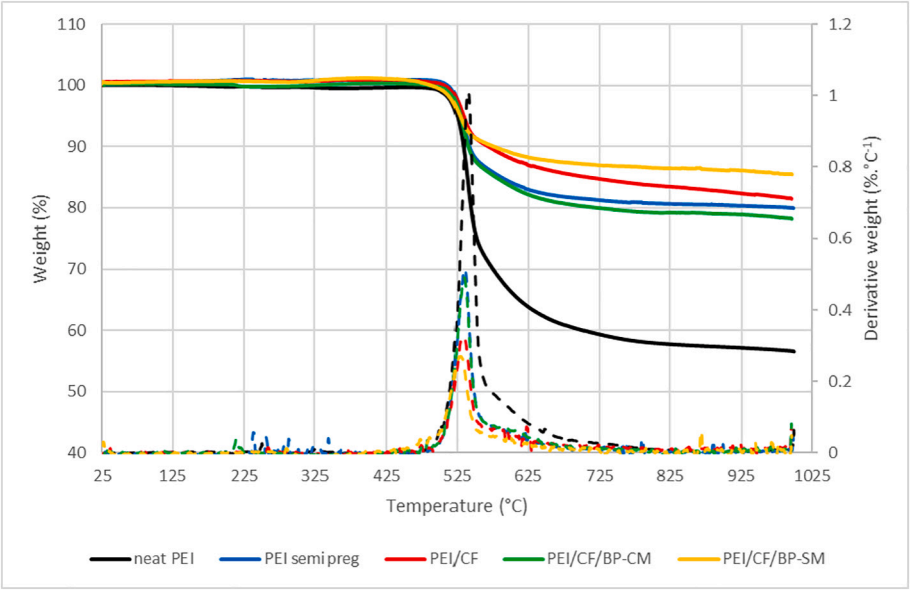

Fig. 6. Weight (solid line) and derivative weight (dash line) curves for PEI-based composites.

mentioning that the PEI semipreg presented a T_i of 470 °C. These values demonstrate the excellent thermal stability of the material. According to the literature [72–74], the PEI decomposition occurs mainly due to the imide group's division and the methyl groups of the isopropylidene unit on the part of the bisphenol A, which contains the most unstable hydrogen atoms (H). The degradation of the material results in the formation of a wide variety of products, such as aromatic and aliphatic ketones, anhydrides, and hydroxyls.

The incorporation of the buckypaper with PEI mats promoted an increase of 10 °C in T_i and an increase of 5 °C in the maximum degradation temperature (T_p) (obtained from the peak temperature in the DTG curve), which suggests an increase of the thermal stability of the material. On the other hand, for BP composite with no PEI mats included a reduction of T_i and T_p (28 °C and 2 °C, respectively) was observed. Such behavior suggests an increase in the thermal stability of the PEI/CF/BP-CM by incorporating the nanostructured film of MWCNT with electrospun PEI mats. The use of PEI mats, as shown in Fig. 3e, showed that the formation of the buckypaper occurred between the polymeric fibers. Therefore, the nanopores that usually make impregnation difficult were filled with polymers favoring the impregnation and optimizing the semipreg and buckypaper interface. Also, the tubes' carboxylic functionalization contributed to improving the interaction with PEI, resulting in laminate with good thermal properties. The final degradation temperature of PEI laminates occurred at approximately 800 °C, with about 80% of waste, in materials that present carbon fiber and 58% for the neat polymer.

The PAEK laminates presented a similar behavior concerning thermal decomposition with at least one thermal decomposition step, which occurs between 500 °C and 750 °C, revealing thus their excellent thermal stability at high temperatures. The PAEK thermoplastic matrix belongs to the poly(ketone) family, as well as the poly (ether ether ketone) (PEEK), poly (ether ketone ketone) (PEKK), and poly (ether ketone) PEK

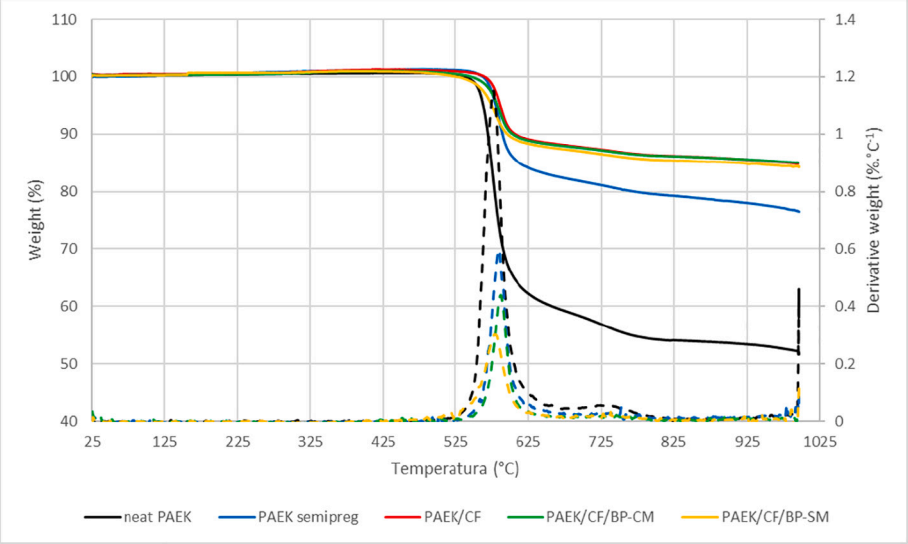

Fig. 7. Weight (solid line) and derivative weight (dash line) curves for PAEK-based composites.

Table 2
Summary of results obtained by TGA, and DMA for PEI compounds materials.

	Neat PEI	PEI Semipreg	PEI/CF	PEI/CF/ BP-CM	PEI/CF/ BP-SM
Initial temperature (T_i)	475 °C	470 °C	470 °C	480 °C	442 °C
Peak temperature (T_p)	540 °C	536 °C	532 °C	537 °C	530 °C
Final temperature (T_f)	800 °C	800 °C	800 °C	800 °C	800 °C
Residue (at 800 °C)	58%	81%	84%	80%	86%
T_g (by tan δ)	–	–	205 °C	214 °C	202 °C
E' (on 30 °C)	–	–	11GPa	8.2GPa	10GPa
E" (on 30 °C)	–	–	0.13GPa	0.11GPa	0.12GPa
Tan δ (on T_g)	–	–	0.57	0.36	0.25

Table 3
Summary results obtained by TGA, DSC, and DMA for PAEK compounds materials.

	Neat PAEK	PAEK semipreg	PAEK/ CF	PAEK/ CF/ BP-CM	PAEK/ CF/ BP-SM
Initial Temperature (T_i)	512 °C	500 °C	500 °C	500 °C	474 °C
Peak temperature (T_p)	568 °C	584 °C	587 °C	586 °C	579 °C
Final temperature (T_f)	750 °C	750 °C	750 °C	750 °C	750 °C
Residue (at 800 °C)	44%	78%	86%	86%	85%
Melt temperature	309 °C	309	307 °C	307 °C	300 °C
Crystallization temperature	266 °C	260 °C	256 °C	250 °C	230 °C
T_g (by tan δ)	–	–	157 °C	157 °C	146 °C
E' (on 30 °C)	–	–	13GPa	8,5GPa	11GPa
E" (on 30 °C)	–	–	0.15GPa	0.08GPa	0.10GPa
Tan δ (on T_g)	–	–	0.036	0.040	0.054

polymers. This material's degradation mechanism occurs initially from the fission of the polymeric chain in the ether and ketone bonds. The products derived from the degradation reactions are predominantly phenol with lower amounts of other compounds such as benzene and dibenzofuran [68–70]. The PAEK/CF composite (reference) showed T_i and T_p of 500 °C and 587 °C, respectively. The incorporation of BP/PEI mats presented no significant variation in T_i and T_p parameters. However, the incorporation of BP with no PEI mats demonstrated both a reduction for T_i and T_p (26 °C and 8 °C, respectively). The final decomposition temperature for both laminates occurred around 750 °C, with a residue ranging between 78% and 86% for materials with carbon fiber and 44% for neat PAEK. PAEK/BP/FC-CM laminate demonstrated that the addition of the BP/PEI promoted no significant changes in the material's thermal stability.

On the other hand, the PEI/FC/BP-CM composite showed reliable results concerning the increase in thermal stability. Díez Pascual et al. [49] presented a 27 °C improvement in T_p for PEEK/BP composites, which demonstrates the significant improvement in the composites' thermal properties by incorporating the CNT film. This behavior can be associated with some factors: the excellent adhesion between the BP and the polymer matrices used in this work hinders the diffusion of the degradation products, thus delaying the decomposition process of the laminates; the covalent bonds between BP (MWCNT-COOH) and polymer matrices restricted the mobility of chains, hence increasing the barrier effect (when added to polymeric matrices, MWCNT can preventively act as barriers during the decomposition process, preventing the transport of decomposed volatile products, thus increasing the thermal stability of the matrix); the high thermal conductivity of the MWCNT facilitates the heat dissipation inside the composite, increasing the material degradation temperature [49,71–73].

PEI and PAEK-base composites with BP presented a reduction in thermal stability, a fact that may be associated with the low permeability of the CNT film. As previously discussed in the literature [74], the through-thickness permeability of the BP is around 10^{-17} to 10^{-19} m^2, which is 4–6 orders of magnitude lower than conventional fiber reinforcements. The small pore size of the CNT film (100–200 nm) was not large enough to allow the polymers to efficiently flow to inside the CNT structure, weakening the interfacial adhesion of the composite, which revealed a worst thermal degradation performance of the laminates compared to BP/PEI samples. Poor interfacial adhesion will probably result in heat transport through phonons and the ineffective barrier effect, therefore reducing material stability.

In addition to the thermostability behavior, an essential property for

semi crystalline thermoplastics, such as PAEK, is crystallization that plays a fundamental role and impacts the material's final properties. The results obtained from the DSC analyzes for PAEK are presented in Fig. 8 and summarized in Table 3. The addition of BP promoted no changes in the melting temperature of the material, except for PAEK/FC/BP-SM, that there was a reduction of 7 °C compared to the reference material (PAEK/CF). Also an exothermic peak was observed for PAEK semipreg at approximately 185 °C, which corresponds to crystallization in heating (hot crystallization). This thermal event occurs due to a very rapid cooling performed during the semipregs processing that prohibits a complete material's crystallization to occur, so that when it is heated again, the material crystallization process occurs. Below the glass transition, molecular mobility is very restricted, and hot crystallization does not occur, but small crystallites are formed during heating above T_g. It is noteworthy that since the semipreg is not the final product, there were no problems in performing rapid cooling. The most critical point here is to control the cooling during the final processing of the material [75,76].

Considering the crystallization temperatures (T_c), a reduction was observed from 256 °C (PAEK/CF) to 250 °C (PAEK/CF/BP-CM) and 230 °C (PAEK/CF/BP-SM) due to the incorporation of BP. A similar observation was done by Díez-Pascual et al. [49], who reported that the addition of BP promoted a reduction of 8 °C and 7 °C in the melting temperature and a reduction of 8 °C and 16 °C in crystallization temperature of PPS and PEEK, respectively. However, some data available in the literature seems to contradict to this. Gohn et al. [77] showed that the addition of CNT promoted an increase in the crystallization temperature in the four different concentrations and Valentini et al. [78] demonstrated that incorporating single-walled carbon nanotube (SWCNT) favored the nucleation process, thus increasing the material's crystallization temperature.

Generally, carbonaceous nanoparticles act as a nucleating agent favoring the polymeric' chain restriction. However, the presence of agglomerates or weak interfacial adhesion reduces the surface contact area between the nanoparticle and matrix, consequently impacting the reduction of the crystallization temperature [48,79]. Besides, lower crystallization temperatures favor the formation of smaller and imperfect crystallites, consequently reducing the melting temperature. For the laminate with BP/PEI mats the reduction in T_c was not that significant, only 6 °C. Although, the laminate with BP had a reduction of 26 °C that possibly impacted the reduction in T_m with a drop of 7 °C. Such reduction may be associated with the polymer chain's favoring mobility caused by the addition of BP due to the weak connections between the graphene layers by the van der Waals forces, allowing the mobility of the polymeric chain within the layers. Besides, the polymer segments crystallized at lower temperatures, impacting the formation of smaller and more imperfect crystals, thus influencing the material's final properties [49].

3.4. Viscoelastic properties of nanostructured composites

DMA analysis is a crucial characterization technique that provides information on viscoelastic properties, usually through the storage modulus (E'), loss modulus (E") and damping factor (Tan δ), and also allows the calculation of entanglement degree and factors A, b and C. The data obtained from this analysis allows to study the interfacial behavior, which determines the composites' performance. The storage modulus and damping factor for PEI and PAEK-based composites are presented in Fig. 9 and the values of E', E" and Tan δ were compiled in Tables 2 and 3.

The incorporation of BP/PEI mat and BP led to a storage modulus reduction of about 30% and 15% for PAEK/CF/BP-CM and PAEK/CF/BP-SM composites, respectively. The same trend was observed for PEI composites revealing a decrease of 25% and 15% for PEI/FC/BP-CM and PEI/CF/BP-SM composites. Once E' is correlated with the material's stiffness, it can be assumed that BP's incorporation promoted a decrease in this parameter for all laminates. Therefore, the stiffness reduction suggests a toughening effect, i.e. a transition in the laminate behavior from a rigid and hard material to a flexible and soft one. As described in the literature [86–88], this behavior is strongly related to the composites' greater energy absorption. This hypothesis will be discussed later based on data from the other factors that were studied.

The PEI/CF and PAEK/CF laminates exhibited an intense peak in tan δ curves corresponding to the respective composites' T_g. The incorporation of BP in the laminates reduced the T_g of the PEI/CF/BP-SM (2%) and PAEK/CF/BP-SM (7%) laminates, whereas for the PEI/CF/BP-CM composites, there was an increase of 5% and no variation was found for PAEK/CF/BP-CM. Several works available in the literature showed [33,48], in general, an increase of T_g due to the BP addition in composites, suggesting a strong restriction on the polymer chain, a fact observed for PEI/CF/BP-CM laminate. The T_g reduction for PEI/CF/BP-SM and PAEK/CF/BP-SM is due to the poor buckypaper impregnation generating a weak interface, thus the buckypaper does not act hindering the polymer's chain mobility. Also, the height of the tan δ peak for both nanostructured systems was smaller compared to the reference laminates (PEI/CF and PAEK/CF). Such behavior suggests that the incorporation of BP promoted a lower energy dissipation of the material, resulting in the reduction of tan δ peaks.

As widely discussed in the literature, the properties of CNT/polymer composites can be negatively affected by the agglomeration of the particles, an issue that can be solved using the buckypaper [80,81]. However, the low permeability of the CNT film compared to conventional fiber reinforcements compromises the CNT network's

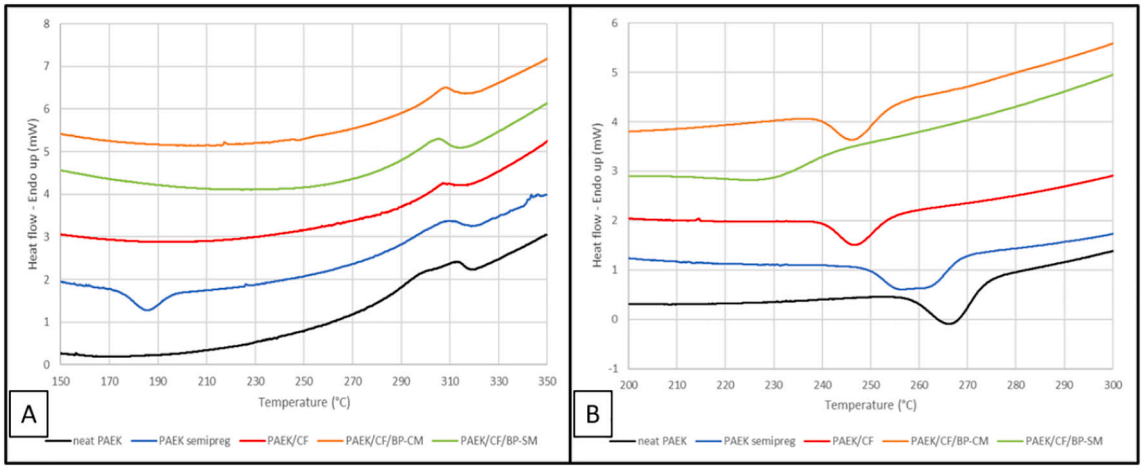

Fig. 8. DSC curves obtained during (a) first heating, and (b) cooling for PAEK polymer matrix materials.

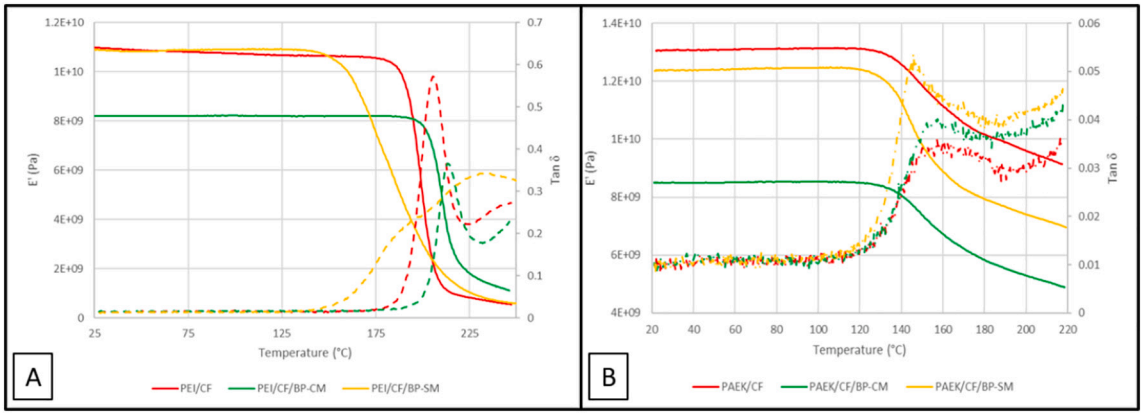

Fig. 9. E' (solid line) and Tan δ (dash line) curve for (a) PEI and (b) PAEK-based composites obtained by DMA.

impregnation by the matrix, thus reducing adhesion between the BP and the polymer employed. According to Fig. 9, the addition of BP and BP/PEI mats promoted a reduction in storage modulus of the composite, whereas this behavior was more significant for the laminates in which the BP was filtered with PEI mats as a substrate. This result indeed suggests a toughening effect of the composites due to incorporating the BP/PEI films.

Based on E' data, the entanglement degree (N) values were

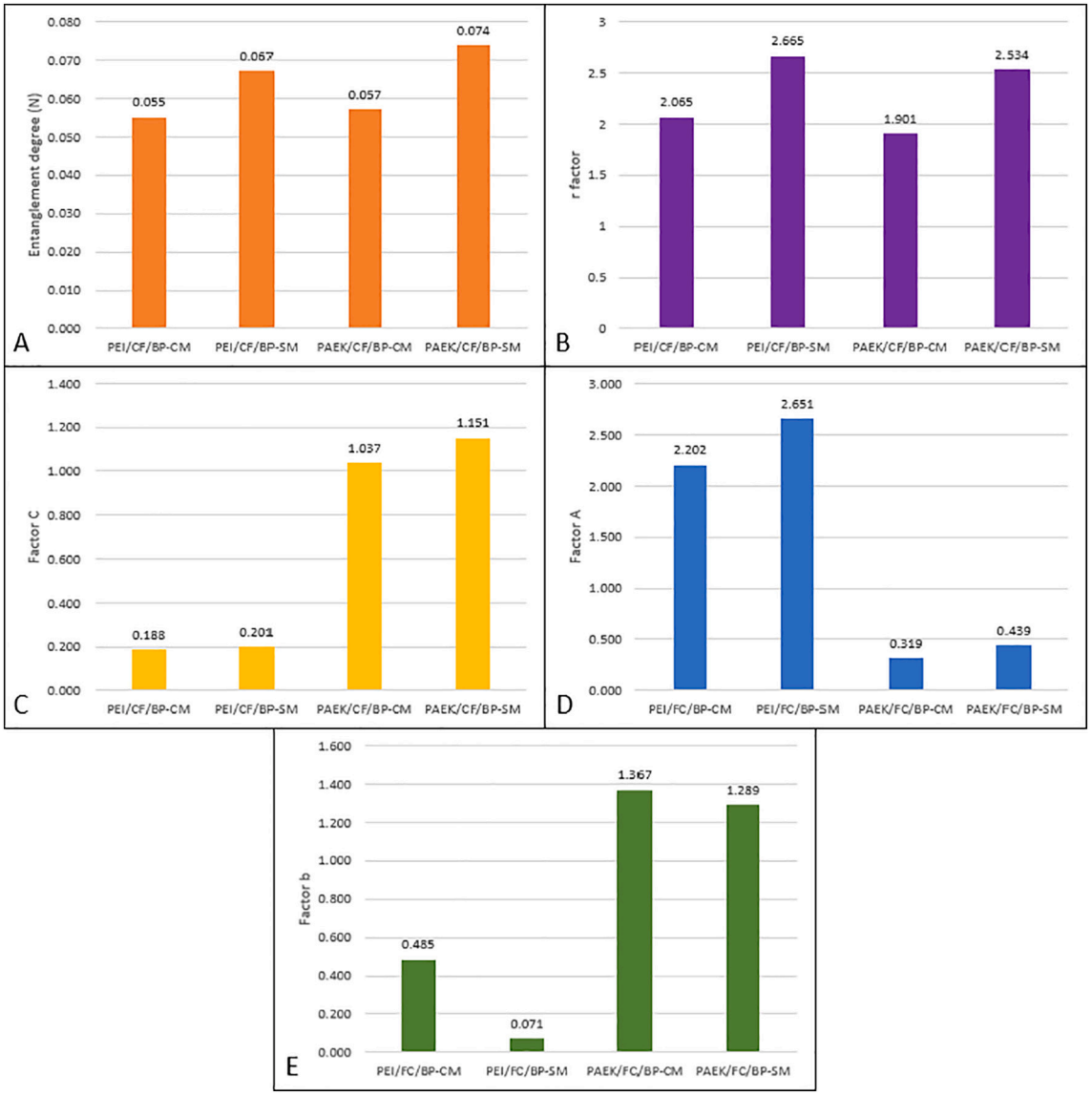

Fig. 10. (a) Entanglement degree; (b) Factor r; (c) Factor C; (d) Factor A; and (e) Factor b for the studied composites.

calculated according to Eq. (1) for all BP composites at glassy region and are shown in Fig. 10a. This parameter is proportional to the reinforcement contribution of carbon nanotubes buckypapers on the viscoelastic properties. The highest N values were 0.074 and 0.067 for PAEK/CF/BP-SM and PEI/CF/BP-SM, respectively, whereas the lowest were 0.057 and 0.055 for PAEK/CF/BP-CM and PAEK/CF/BP-CM, respectively. The highest values obtained for laminates without PEI mats indicate that nanoparticles tend to have less interaction among them than BP/PEI mats, thus contributing to enhance the E'.

The results obtained for factor r (reinforcement efficiency) at the studied composites' glassy region were calculated from Eq. (2) and the results compiled in Fig. 10b. Behavior similar to the degree of entanglement (N) was observed for factor r. Therefore, the laminates PEI/CF/BP-SM and PAEK/CF/BP-SM obtained the highest values of 2.665 and 2.534, respectively, followed by the lowest values of 2.065 and 1.901 for PEI/CF/BP-CM and PAEK/CF/BP-CM, respectively. The results concluded that the composites with BP without PEI mats obtained a better filler matrix bonding. The degree of entanglement and the factor have the same E' trend since both parameters are dependent on E,' and the volumetric fraction of carbon nanotubes remains the same for all composites produced. Therefore, the other factors A, b, and C will provide important information to understand the real contribution of buckypapers with and without PEI mats.

The "C" factor provides information of the BP effectiveness in the glassy region (Fig. 10c), and once it is associated with the storage modulus, this factor is sensitive to the reduction of E' during the increase of the temperature. The glass transition temperature is an essential parameter for evaluating polymer systems because it helps to determine the material's temperature application. It is well known that below the T_g, the polymer chains have relatively little mobility. As reported by several authors [49,82–84], the addition of CNT tends to restrict the polymer chains' mobility, increasing the glass transition temperature of the laminates. The "C" parameter determines the BP contribution in the composite's glass transition temperature, thus low values indicate high efficiency and proficiency in the nanoparticles distribution [41,44]. The lowest values obtained for "C" were 0.19 and 1.04 for PEI/CF/BP-CM and PAEK/CF/BP-CM, respectively, which consolidates BP/PEI mats effectiveness. This behavior was observed due to the increase of the glass transition temperature of the PEI/CF/BP-CM laminate.

Aside from the variables associated with the storage modulus, two parameters obtained from Tan δ contribute to understanding the influence of BPs on viscoelastic properties. The first parameter is factor "A" or adhesion factor (Fig. 10d) provides information regarding the polymer/nanoparticle interactions, hence strong interactions between nanoparticles and matrix in the interface region reduces the macromolecular mobility next to nanoparticles surfaces. PEI/CF/BP-CM (2.20) and PAEK/CF/BP-CM (0.32) samples have the lowest values, which suggest strong interactions between the components when PEI mats are added. Furthermore, the interactions become less dependent on the temperature as the factor "A" is reduced.

The last parameter studied in this work is the dissipation factor (b). According to Sarasua and Pouyet [71], Pandey et al. [43] and the dynamic mechanical analysis can provide information about polymer-fiber interphase, taking into account that the material dissipation does not depend only on the polymeric matrix but also on interfaces and interactions that form layers of the interphases between the fiber and the matrix. The "b" factor values are shown in Fig. 10e. According to [71], the weak interphase occurs for $b < 0$ and the strong interphase for $b > 0$. The laminates of PEI/CF/BP-CM (0.485) and PAEK/CF/BP-CM (1367) obtained the highest values for "b" factor, thus indicating that the addition of BP/PEI mats favors the formation of a region wider of restraining interphase layer than BP without PEI mats. Therefore, BP/PEI mats in PEI and PAEK laminates contribute more significantly to the micromechanical stress distribution due to the restraining interphase layer [44].

The nanoparticles dispersion and the polymer/CNT interface are the keys to achieving a gain in properties for nanostructured composites. Nevertheless, as the incorporation of CNT in this work was based on buckypapers, interfacial adhesion and its strength is the main factor to be studied [15]. Theoretically, the addition of CNTs in a polymeric matrix restricts the movement of the polymeric chains, increasing the material stiffness and reducing the material ductility [48]. Therefore, DMA data suggest the composite toughening, since the addition of buckypaper, mainly with PEI mats, favored the mobility of the polymeric chain and reducing storage modulus which is associated with the materials' stiffness. The other parameters studied (degree of entanglement and factors A, b, C, and r) show that BP/PEI mats, despite having lower N and r factor values, which suggests a more significant interaction between nanotubes and the formation of clusters, which was not observed in buckypapers morphology and lower nanoparticles matrix bonding. BP/PEI mats promotes a more outstanding contribution in passing through the glass transition in both materials; besides generating a more significant interaction between the composites' constituents and the presence of a larger region of interphase, it will contribute to a better micromechanical distribution.

4. Conclusions

This work proposed a systematic study to achieve the best processing conditions for buckypapers and proposing the use of PEI mats to facilitate the handling and matrix/buckypaper adhesion. Based on the time and amplitude parameters previously defined by Rojas et al., the processed BP with the highest power (100 W) presented the best features to be incorporated in the laminates, showing high porosity, low defects, and a better crystalline structure. The electrospinning proved to be an efficient method to prepare PEI mats showing good quality to be applied as a BP substrate. The thermal stability of both PEI and PAEK composites showed no significant variation by incorporating BP/PEI mats. However, it is essential to point out that a small reduction in the PAEK composite's crystallization temperature was observed due to the incorporation of BP/PEI mats. Furthermore, incorporating the BP/PEI film promoted a toughening effect in the composites, revealing a proper absorption of energy capacity by the material. Based on the detailed study carried out in this work, it can be concluded that PAEK and PEI composites are suitable for aeronautical applications that demand to absorb impacts and have high interlaminar resistance values.

CRediT authorship contribution statement

Luis Felipe de Paula Santos: Conceptualization, Methodology, Validation, Investigation, Writing – original draft. **René Alderliesten:** Validation, Writing – review & editing, Supervision. **Winand Kok:** Validation, Writing – review & editing, Resources. **Bruno Ribeiro:** Conceptualization, Methodology, Validation, Writing – review & editing, Supervision. **Juliana Bovi de Oliveira:** Conceptualization, Methodology, Validation. **Michelle Leali Costa:** Conceptualization, Validation, Writing – review & editing, Supervision. **Edson Cocchieri Botelho:** Conceptualization, Validation, Writing – review & editing, Supervision.

Declaration of competing interest

The authors certify that they have NO affiliations with or involvement in any organization or entity with any financial interest (such as honoraria; educational grants; participation in speakers' bureaus; membership, employment, consultancies, stock ownership, or other equity interest; and expert testimony or patent-licensing arrangements), or non-financial interest (such as personal or professional relationships, affiliations, knowledge or beliefs) in the subject matter or materials discussed in this manuscript.

Acknowledgements

The authors are grateful for all support given by Delft University of Technology and the financial support given by the Brazilian Funding Institutions: São Paulo Foundation Research (FAPESP) (2017/16970-0; 2017/04740-0, 2018/07867-3 and 2019/18691-6), National Council for Scientific and Technological Development (CNPq) (140852/2018-2, 306576/2020-1 and 304876/2020-8) and this study was financed in part by the Coordenação de Aperfeiçoamento de Pessoal de Nível Superior – Brasil (CAPES) – Finance Code 001. Also, the authors are grateful for Nanografi for donating the carbon nanotubes and Toray Advanced Composites for the semipregs used in this work.

References

[1] M. Ducousso, A. Dalodière, A. Baillard, Evaluation of the thermal aging of aeronautical composite materials using Lamb waves, Ultrasonics. 94 (2019) 174–182, https://doi.org/10.1016/j.ultras.2018.09.014.
[2] M.S.A. Majid, J.S. Mandeep, K.A. Ahmad, Performance analysis of composite ply orientation vehicle (UAV) NACA4415 wing, Integr. Med. Res. (2019) 1–13, https://doi.org/10.1016/j.jmrt.2019.06.044.
[3] S. Russo, P. Lamberti, M. Zarrelli, L. Guadagno, G. Iannuzzo, L. Vertuccio, G. Spinelli, Smart coatings of epoxy based CNTs designed to meet practical expectations in aeronautics, Compos. Part B Eng. 147 (2018) 42–46, https://doi.org/10.1016/j.compositesb.2018.04.027.
[4] K.K. Sairajan, G.S. Aglietti, K.M. Mani, A review of multifunctional structure technology for aerospace applications, Acta Astronaut. 120 (2016) 30–42, https://doi.org/10.1016/j.actaastro.2015.11.024.
[5] D.D.L. Chung, A review of multifunctional polymer-matrix structural composites, Compos. Part B Eng. 160 (2019) 644–660, https://doi.org/10.1016/j.compositesb.2018.12.117.
[6] W. Ye, W. Wu, X. Hu, G. Lin, J. Guo, H. Qu, J. Zhao, 3D printing of carbon nanotubes reinforced thermoplastic polyimide composites with controllable mechanical and electrical performance, Compos. Sci. Technol. 182 (2019) 107671, https://doi.org/10.1016/j.compscitech.2019.05.028.
[7] D. Ren, Y. Chen, H. Li, H.U. Rehman, Y. Cai, H. Liu, High-efficiency dual-responsive shape memory assisted self-healing of carbon nanotubes enhanced polycaprolactone/ thermoplastic polyurethane composites, Colloids Surf. A Physicochem. Eng. Asp. 580 (2019) 123731, https://doi.org/10.1016/j.colsurfa.2019.123731.
[8] W.J. Sun, L. Xu, L.C. Jia, C.G. Zhou, Y. Xiang, R.H. Yin, D.X. Yan, J.H. Tang, Z. M. Li, Highly conductive and stretchable carbon nanotube/thermoplastic polyurethane composite for wearable heater, Compos. Sci. Technol. 181 (2019) 107695, https://doi.org/10.1016/j.compscitech.2019.107695.
[9] V. Dhand, W.R. Lee, S.-J. Park, K.Y. Rhee, G. Mittal, A review on carbon nanotubes and graphene as fillers in reinforced polymer nanocomposites, J. Ind. Eng. Chem. 21 (2014) 11–25, https://doi.org/10.1016/j.jiec.2014.03.022.
[10] L. Peponi, D. Puglia, L. Torre, L. Valentini, J.M. Kenny, Processing of nanostructured polymers and advanced polymeric based nanocomposites, Mater. Sci. Eng. R. 85 (2014) 1–46, https://doi.org/10.1016/j.mser.2014.08.002.
[11] P. Tadini, N. Grange, K. Chetehouna, N. Gascoin, S. Senave, I. Reynaud, Thermal degradation analysis of innovative PEKK-based carbon composites for high-temperature aeronautical components, Aerosp. Sci. Technol. 65 (2017) 106–116, https://doi.org/10.1016/j.ast.2017.02.011.
[12] M. Ashuri, Q. He, Y. Liu, S. Emani, L.L. Shaw, Synthesis and performance of nanostructured silicon/graphite composites with a thin carbon shell and engineered voids, Electrochim. Acta 258 (2017) 274–283, https://doi.org/10.1016/j.electacta.2017.10.198.
[13] A.M. Vorobei, O.I. Pokrovskiy, K.B. Ustinovich, O.O. Parenago, S.V. Savilov, V. V. Lunin, V.M. Novotortsev, Preparation of Polymer E Multi-walled Carbon Nanotube Composites with Enhanced Mechanical Properties Using Supercritical Antisolvent Precipitation 95, 2016, pp. 77–81.
[14] B. Ribeiro, E.C. Botelho, M.L. Costa, C.F. Bandeira, Carbon nanotube buckypaper reinforced polymer composites: a review, Polímeros 27 (2017) 247–255, https://doi.org/10.1590/0104-1428.03916.
[15] J. Chen, L. Yan, W. Song, D. Xu, Interfacial characteristics of carbon nanotube-polymer composites: a review, Compos. Part A Appl. Sci. Manuf. 114 (2018) 149–169, https://doi.org/10.1016/j.compositesa.2018.08.021.
[16] B. Qu, D. Zhuo, R. Wang, L. Wu, X. Cheng, Enhancement of mechanical properties of buckypapers/polyethylene composites by microwave irradiation, Compos. Sci. Technol. 164 (2018) 313–318, https://doi.org/10.1016/j.compscitech.2018.06.002.
[17] J.A. Rojas, L.F.P. Santos, M.L. Costa, B. Ribeiro, E.C. Botelho, Moisture and temperature influence on mechanical behavior of PPS / buckypapers carbon fiber laminates, Mater. Res. Express. 4 (2017) aa797c, https://doi.org/10.1088/2053-1591/aa797c.
[18] J.A. Rojas, L.A. Ardila-Rodríguez, M.F. Diniz, M. Gonçalves, B. Ribeiro, M. C. Rezende, Optimization of Triton X-100 removal and ultrasound probe parameters in the preparation of multiwalled carbon nanotube buckypaper, Mater. Des. 166 (2019) 107612, https://doi.org/10.1016/j.matdes.2019.107612.
[19] F. Pons, J. Cinquin, Enhancement of Electrical Conductivity of Composite Structures by Integration of Carbon Nanotubes Via Bulk Resin and / or Buckypaper Films 122, 2017, pp. 31–40.
[20] J.A. Rojas, B. Ribeiro, M.C. Rezende, Influence of serrated edge and rectangular strips of MWCNT buckypaper on the electromagnetic properties of glass fiber/epoxy resin composites, Carbon N.Y. 160 (2020) 317–327, https://doi.org/10.1016/j.carbon.2020.01.036.
[21] G. Trakakis, G. Anagnostopoulos, L. Sygellou, A. Bakolas, J. Parthenios, D. Tasis, C. Galiotis, K. Papagelis, Epoxidized multi-walled carbon nanotube buckypapers: a scaffold for polymer nanocomposites with enhanced mechanical properties, Chem. Eng. J. 281 (2015) 793–803, https://doi.org/10.1016/j.cej.2015.06.085.
[22] P.E. Lopes, F. van Hattum, C.M.C. Pereira, P.J.R.O. Nóvoa, S. Forero, F. Hepp, L. Pambaguian, High CNT content composites with CNT Buckypaper and epoxy resin matrix: impregnation behaviour composite production and characterization, Compos. Struct. 92 (2010) 1291–1298, https://doi.org/10.1016/j.compstruct.2009.11.003.
[23] L. Cafiero, S. Iannace, L. Sorrentino, Microcellular foams from high performance miscible blends based on PEEK and PEI, Eur. Polym. J. 78 (2016) 116–128, https://doi.org/10.1016/j.eurpolymj.2016.03.014.
[24] M.K. Pitchan, S. Bhowmik, M. Balachandran, M. Abraham, Process optimization of functionalized MWCNT/polyetherimide nanocomposites for aerospace application, Mater. Des. 127 (2017) 193–203, https://doi.org/10.1016/j.matdes.2017.04.081.
[25] K.V. Mahesh, S. Balanand, R. Raimond, A. Peer Mohamed, S. Ananthakumar, Polyaryletherketone polymer nanocomposite engineered with nanolaminated Ti3SiC2ceramic fillers, Mater. Des. 63 (2014) 360–367, https://doi.org/10.1016/j.matdes.2014.06.034.
[26] G.C. Papanicolaou, S.P. Zaoutsos, Viscoelastic Constitutive Modeling of Creep and Stress Relaxation in Polymers and Polymer Matrix Composites, 2nd ed., Elsevier Ltd., 2019 https://doi.org/10.1016/b978-0-08-102601-4.00001-1.
[27] J. Zhang, D. Jiang, Composites: Part A Influence of Geometries of Multi-walled Carbon Nanotubes on the Pore Structures of Buckypaper 43, 2012, pp. 469–474, https://doi.org/10.1016/j.compositesa.2011.11.016.
[28] A.M. Díez-Pascual, M. Naffakh, C. Marco, G. Ellis, Mechanical and electrical properties of carbon nanotube/poly(phenylene sulphide) composites incorporating polyetherimide and inorganic fullerene-like nanoparticles, Compos. Part A Appl. Sci. Manuf. 43 (2012) 603–612, https://doi.org/10.1016/j.compositesa.2011.12.026.
[29] B. Beylergil, M. Tanoğlu, E. Aktaş, Enhancement of interlaminar fracture toughness of carbon fiber–epoxy composites using polyamide-6,6 electrospun nanofibers, J. Appl. Polym. Sci. 134 (2017), https://doi.org/10.1002/app.45244.
[30] H. Ipackchi, A.M. Rezadoust, M. Esfandeh, M. Rezaei, Improvement of interlaminar fracture toughness of phenolic laminates interleaved with electrospun polyvinyl butyral nano fi bers, Theor. Appl. Fract. Mech. 105 (2020) 102406, https://doi.org/10.1016/j.tafmec.2019.102406.
[31] B. Ribeiro, J.A.R. Corredor, L. Ardila, L.F.P. Santos, M.L. Costa, M.C. Rezende, E. C. Botelho, Preparation, thermal and mechanical properties of poly (ether-imide) composite reinforced with carbon nanotube buckypaper, J. Appl. Polym. Sci. 137 (2020) 1–8, https://doi.org/10.1002/app.48330.
[32] H. Chen, V.V. Ginzburg, J. Yang, Y. Yang, W. Liu, Y. Huang, L. Du, B. Chen, Progress in Polymer Science Thermal conductivity of polymer-based composites : Fundamentals and applications, Prog. Polym. Sci. 59 (2016) 41–85, https://doi.org/10.1016/j.progpolymsci.2016.03.001.
[33] X. Xiong, Y. Zeng, R. Ren, S. Liu, S. Lu, P. Chen, Preparation and thermal properties of soluble poly(phthalazinone ether sulfone ketone) composites reinforced with multi-walled carbon nanotube buckypaper, Compos. Part A Appl. Sci. Manuf. 89 (2016) 2–9, https://doi.org/10.1016/j.compositesa.2016.06.001.
[34] L.R. Manea, E. Nechita, I. Sandu, Electrospinning of polyetherimide (PEI) solution: effect of nozzle sizes on the diameter of the fiber, Rev. Chim. 66 (2015) 1841–1845.
[35] D.M. Sato, L.M. Guerrini, M.P. De Oliveira, L.R.D.O. Hein, E.C. Botelho, Production and characterization of polyetherimide mats by an electrospinning process, Mater. Res. Express. 5 (2018), https://doi.org/10.1088/2053-1591/aadd85.
[36] J. Han, H. Zhang, M. Chen, D. Wang, Q. Liu, The Combination of Carbon Nanotube Buckypaper and Insulating Adhesive for Lightning Strike Protection of the Carbon Fiber / Epoxy Laminates 4, 2015.
[37] L. Liu, L. Shen, Y. Zhou, Improving the interlaminar fracture toughness of carbon/epoxy laminates by directly incorporating with porous carbon nanotube buckypaper, J. Reinf. Plast. Compos. 35 (2016) 165–176, https://doi.org/10.1177/0731684415610919.
[38] Z. Oommen, G. Groeninckx, S. Thomas, Dynamic mechanical and thermal properties of physically compatibilized natural rubber/poly(methyl methacrylate) blends by the addition of natural rubber-graft-poly(methyl methacrylate), J. Polym. Sci. Part B Polym. Phys. 38 (2000) 525–536, https://doi.org/10.1002/(SICI)1099-0488(20000215)38:4<525::AID-POLB4>3.0.CO;2-T.
[39] Z. Oommen, G. Groeninckx, S. Thomas, Dynamic mechanical and thermal properties of physically compatibilized natural rubber/poly(methyl methacrylate) blends by the addition of natural rubber-graft-poly(methyl methacrylate), J. Polym. Sci. Part B Polym. Phys. 38 (2000) 525–536, https://doi.org/10.1002/(SICI)1099-0488(20000215)38:4<525::AID-POLB4>3.0.CO;2-T.
[40] J. Jyoti, B.P. Singh, A.K. Arya, S.R. Dhakate, Dynamic mechanical properties of multiwall carbon nanotube reinforced ABS composites and their correlation with entanglement density, adhesion, reinforcement and C factor, RSC Adv. 6 (2016) 3997–4006, https://doi.org/10.1039/c5ra25561a.
[41] N. Hameed, P.A. Sreekumar, B. Francis, W. Yang, S. Thomas, Morphology, dynamic mechanical and thermal studies on poly(styrene-co-acrylonitrile) modified epoxy

resin/glass fibre composites, Compos. Part A Appl. Sci. Manuf. 38 (2007) 2422–2432, https://doi.org/10.1016/j.compositesa.2007.08.009.
[42] D. Romanzini, H.L. Ornaghi, S.C. Amico, A.J. Zattera, Influence of fiber hybridization on the dynamic mechanical properties of glass/ramie fiber-reinforced polyester composites, J. Reinf. Plast. Compos. 31 (2012) 1652–1661, https://doi.org/10.1177/0731684412459982.
[43] A.K. Pandey, T. Pal, R. Sharma, K.K. Kar, Study of matrix–filler interaction through correlations between structural and viscoelastic properties of carbonous-filler/polymer-matrix composites, J. Appl. Polym. Sci. 137 (2020) 1–16, https://doi.org/10.1002/app.48660.
[44] A.K. Pandey, R. Kumar, V.S. Kachhavah, K.K. Kar, Mechanical and thermal behaviours of graphite flake-reinforced acrylonitrile-butadiene-styrene composites and their correlation with entanglement density, adhesion, reinforcement and: C factor, RSC Adv. 6 (2016) 50559–50571, https://doi.org/10.1039/c6ra09236e.
[45] J. Kubát, M. Rigdahl, M. Welander, Characterization of interfacial interactions in high density polyethylene filled with glass spheres using dynamic-mechanical analysis, J. Appl. Polym. Sci. 39 (1990) 1527–1539, https://doi.org/10.1002/app.1990.070390711.
[46] A.K. Pandey, K. Singh, K.K. Kar, Thermo-mechanical properties of graphite-reinforced high-density polyethylene composites and its structure–property corelationship, J. Compos. Mater. 51 (2017) 1769–1782, https://doi.org/10.1177/0021998316683782.
[47] S. Qu, Y. Dai, D. Zhang, Q. Li, T.-W. Chou, W. Lyu, Carbon nanotube film based multifunctional composite materials: an overview, Funct. Compos. Struct. 2 (2020), 022002, https://doi.org/10.1088/2631-6331/ab9752.
[48] A.M. Díez-Pascual, J. Guan, B. Simard, M.A. Gómez-Fatou, Poly(phenylene sulphide) and poly(ether ether ketone) composites reinforced with single-walled carbon nanotube buckypaper: II - mechanical properties, electrical and thermal conductivity, Compos. Part A Appl. Sci. Manuf. 43 (2012) 1007–1015, https://doi.org/10.1016/j.compositesa.2011.11.003.
[49] A.M. Díez-Pascual, J. Guan, B. Simard, M.A. Gómez-Fatou, Poly(phenylene sulphide) and poly(ether ether ketone) composites reinforced with single-walled carbon nanotube buckypaper: I – structure, thermal stability and crystallization behaviour, Compos. Part A Appl. Sci. Manuf. 43 (2012) 997–1006, https://doi.org/10.1016/j.compositesa.2011.11.002.
[50] K. Kobashi, H. Yoon, S. Ata, T. Yamada, D.N. Futaba, K. Hata, Designing neat and composite carbon nanotube materials by porosimetric characterization, Nanoscale Res. Lett. 12 (2017), https://doi.org/10.1186/s11671-017-2384-2.
[51] R.L.D. Whitby, T. Fukuda, T. Maekawa, S.L. James, S.V. Mikhalovsky, Geometric control and tuneable pore size distribution of buckypaper and buckydiscs, Carbon N.Y. 46 (2008) 949–956, https://doi.org/10.1016/j.carbon.2008.02.028.
[52] Y.Y. Huang, E.M. Terentjev, Dispersion of carbon nanotubes: mixing, sonication, stabilization, and composite properties, Polymers (Basel) 4 (2012) 275–295, https://doi.org/10.3390/polym4010275.
[53] R. Saito, M. Hofmann, G. Dresselhaus, A. Jorio, M.S. Dresselhaus, Raman spectroscopy of graphene and carbon nanotubes, Adv. Phys. 60 (2011) 413–550, https://doi.org/10.1080/00018732.2011.582251.
[54] K.K. Singh, S.K. Chaudhary, R. Venugopal, A. Gaurav, Bulk synthesis of multi-walled carbon nanotubes by AC arc discharge method, Proc. Inst. Mech. Eng. Part N J. Nanomater. Nanoeng. Nanosyst. 231 (2017) 141–151, https://doi.org/10.1177/2397791417712836.
[55] Y. Hu, D. Li, P. Tang, Y. Bin, H. Wang, Comparative study of structure, mechanical and electromagnetic interference shielding properties of carbon nanotube buckypapers prepared by different dispersion media, Mater. Des. 293 (2019) 108175, https://doi.org/10.1016/j.matdes.2019.108175.
[56] J.P. Tessonnier, D. Rosenthal, T.W. Hansen, C. Hess, M.E. Schuster, R. Blume, F. Girgsdies, N. Pfänder, O. Timpe, D.S. Su, R. Schlögl, Analysis of the structure and chemical properties of some commercial carbon nanostructures, Carbon N. Y. 47 (2009) 1779–1798, https://doi.org/10.1016/j.carbon.2009.02.032.
[57] H. Murphy, P. Papakonstantinou, T.I.T. Okpalugo, Raman study of multiwalled carbon nanotubes functionalized with oxygen groups, J. Vac. Sci. Technol. B Microelectron. Nanom. Struct. 24 (2006) 715–720, https://doi.org/10.1116/1.2180257.
[58] P. Eduardo, M.C. Rezende, Carbono Polimérico: Processamento e Aplicação, in: Polímeros Ciência e Tecnol., 1998, pp. 22–30.
[59] V.A. da Silva, M.C. Rezende, Effect of the morphology and structure on the microwave absorbing properties of multiwalled carbon nanotube filled epoxy resin nanocomposites, Mater. Res. 21 (2018), https://doi.org/10.1590/1980-5373-mr-2017-0977.
[60] M. Borrotti, E. Lanzarone, F. Manganini, S. Ortelli, A. Pievatolo, C. Tonetti, Defect minimization and feature control in electrospinning through design of experiments, J. Appl. Polym. Sci. 134 (2017) 1–10, https://doi.org/10.1002/app.44740.
[61] A. Haider, S. Haider, I.K. Kang, A comprehensive review summarizing the effect of electrospinning parameters and potential applications of nanofibers in biomedical and biotechnology, Arab. J. Chem. 11 (2018) 1165–1188, https://doi.org/10.1016/j.arabjc.2015.11.015.
[62] L. Cafiero, S. Iannace, L. Sorrentino, Microcellular foams from high performance miscible blends based on PEEK and PEI, Eur. Polym. J. 78 (2016) 116–128, https://doi.org/10.1016/j.eurpolymj.2016.03.014.
[63] M. Iannone, A. D'Amore, Processing of PEEK/PEI Blends for High Performance Composites in Aerospace, 2019, p. 020019, https://doi.org/10.1063/1.5140292.
[64] M. Shibata, Z. Fang, R. Yosomiya, Miscibility and crystallization behavior of poly (ether ether ketone ketone)/poly(ether imide) blends, J. Appl. Polym. Sci. 80 (2001) 769–775, https://doi.org/10.1002/1097-4628(20010502)80:5<769::AID-APP1153>3.0.CO;2-B.
[65] R. Ramani, S. Alam, Composition optimization of PEEK/PEI blend using model-free kinetics analysis, Thermochim. Acta 511 (2010) 179–188, https://doi.org/10.1016/j.tca.2010.08.012.
[66] M. Jenkins, Crystallisation in miscible blends of PEEK and PEI, Polymer (Guildf) 42 (2001) 1981–1986, https://doi.org/10.1016/S0032-3861(00)00438-9.
[67] N.L. Batista, M.L. Costa, K. Iha, E.C. Botelho, Thermal degradation and lifetime estimation of poly(ether imide)/carbon fiber composites, J. Thermoplast. Compos. Mater. 28 (2015) 265–274, https://doi.org/10.1177/0892705713484740.
[68] J.N. Panda, J. Bijwe, R.K. Pandey, Optimization of graphite contents in PAEK composites for best combination of performance properties, Compos. Part B Eng. 174 (2019) 106951, https://doi.org/10.1016/j.compositesb.2019.106951.
[69] G. da Cunha Vasconcelos, R.L. Mazur, E.C. Botelho, M.C. Rezende, M.L. Costa, Evaluation of crystallization kinetics of poly (ether-ketone- ketone) and poly (ether-ether- ketone) by DSC, J. Aerosp. Technol. Manag. 2 (2010) 155–162, https://doi.org/10.5028/jatm.2010.02026310.
[70] P. Patel, T.R. Hull, R.W. McCabe, D. Flath, J. Grasmeder, M. Percy, Mechanism of thermal decomposition of poly(ether ether ketone) (PEEK) from a review of decomposition studies, Polym. Degrad. Stab. 95 (2010) 709–718, https://doi.org/10.1016/j.polymdegradstab. 2010.01.024.
[71] M. Tunckol, E.Z. Hernandez, J.R. Sarasua, J. Durand, P. Serp, Polymerized ionic liquid functionalized multi-walled carbon nanotubes/polyetherimide composites, Eur. Polym. J. 49 (2013) 3770–3777, https://doi.org/10.1016/j.eurpolymj.2013.08.007.
[72] F.V. Ferreira, W. Franceschi, B.R.C. Menezes, F.S. Brito, K. Lozano, A.R. Coutinho, L.S. Cividanes, G.P. Thim, Dodecylamine functionalization of carbon nanotubes to improve dispersion, thermal and mechanical properties of polyethylene based nanocomposites, Appl. Surf. Sci. 410 (2017) 267–277, https://doi.org/10.1016/j.apsusc.2017.03.098.
[73] B. Ribeiro, L.F.P. Santos, A.L. Santos, M.L. Costa, E.C. Botelho, Decomposition kinetic study of multiwalled carbon nanotube buckypaper-reinforced poly(ether-imide) composites, J. Thermoplast. Compos. Mater. 32 (2019) 62–75, https://doi.org/10.1177/0892705717744827.
[74] B. Ribeiro, J.A.R. Corredor, M.L. Costa, E.C. Botelho, M.C. Rezende, Multifunctional characteristics of glass fiber-reinforced epoxy polymer composites with multiwalled carbon nanotube buckypaper interlayer, Polym. Eng. Sci. 60 (2020) 740–751, https://doi.org/10.1002/pen.25332.
[75] J.E. Spruiell, C.J. Janke, S.W. Case, K.L. Reifnider, A Review of the Measurement and Development of Crystallinity and its Relation to Properties in Neat PPS and its Fiber Reinforced Composites, 2004, https://doi.org/10.2172/885940.
[76] G. Vanden Poel, V.B.F. Mathot, High performance differential scanning calorimetry (HPer DSC): a powerful analytical tool for the study of the metastability of polymers, Thermochim. Acta 461 (2007) 107–121, https://doi.org/10.1016/j.tca.2007.04.009.
[77] A.M. Gohn, J. Seo, R.H. Colby, R.P. Schaake, R. Androsch, A.M. Rhoades, Crystal nucleation in poly(ether ether ketone)/carbon nanotube nanocomposites at high and low supercooling of the melt, Polymer (Guildf) 199 (2020) 1–8, https://doi.org/10.1016/j.polymer.2020.122548.
[78] V. Romanov, S.V. Lomov, I. Verpoest, L. Gorbatikh, Inter-fiber stresses in composites with carbon nanotube grafted and coated fibers, Compos. Sci. Technol. 114 (2015) 79–86, https://doi.org/10.1016/j.compscitech.2015.04.013.
[79] M.F. Arif, H. Alhashmi, K.M. Varadarajan, J.H. Koo, A.J. Hart, S. Kumar, Multifunctional performance of carbon nanotubes and graphene nanoplatelets reinforced PEEK composites enabled via FFF additive manufacturing, Compos. Part B Eng. 184 (2020) 107625, https://doi.org/10.1016/j.compositesb.2019.107625.
[80] F. Zahedi, I.A. Amraee, Carboxylated multiwalled carbon nanotubes effect on dynamic mechanical behavior of soft films composed of multilayer polymer structure, Polymer (Guildf) 151 (2018) 187–196, https://doi.org/10.1016/j.polymer.2018.07.044.
[81] J.A. Rojas, L.A. Ardila-Rodríguez, M.F. Diniz, M. Gonçalves, B. Ribeiro, M. C. Rezende, Highly porous multiwalled carbon nanotube buckypaper using electrospun polyacrylonitrile nanofiber as a sacrificial material, Heliyon 5 (2019), e01386, https://doi.org/10.1016/j.heliyon.2019.e01386.
[82] S.C. Her, K.Y. Lin, Dynamic mechanical analysis of carbon nanotube-reinforced nanocomposites, J. Appl. Biomater. Funct. Mater. 15 (2017) S13–S18, https://doi.org/10.5301/jabfm.5000351.
[83] S. Ebnesajjad, Introduction to plastics, in: Chem. Resist. Eng. Thermoplast., Elsevier, 2016: pp. xiii–xxv. doi:https://doi.org/10.1016/B978-0-323-47357-6.00021-0.
[84] R.-M. Wang, S.-R. Zheng, Y.-P. Zheng, Matrix materials, in: Polym. Matrix Compos. Technol, Elsevier, 2011, pp. 101–548, https://doi.org/10.1533/9780857092229.1.101.
[85] Luis Santos F. P., Bruno Ribeiro, Luis Hein R. O., Rene Alderliesten, Dimitrios Zarouchas, Edson Botelho C., Michelle Costa L., The effect of temperature on fatigue strength of poly (ether-imide)/multiwalled carbon nanotube/carbon fiber composites for aeronautical application, J. Appl. Polym. Sci. (2020), https://doi.org/10.1002/app.49160.